Inorganic Chemistry

Article

pubs.acs.org/IC

Synthesis of Nanocrystals and Particle Size Effects Studies on the Thermally Induced Spin Transition of the Model Spin Crossover Compound $[Fe(phen)_2(NCS)_2]$

Francisco Javier Valverde-Muñoz,[†] Ana B. Gaspar,[*,†] Sergii I. Shylin,[‡,§] Vadim Ksenofontov,[‡] and José A. Real[*,†]

[†]Institut de Ciència Molecular/Departament de Química Inorgànica, Universitat de València, C/Catedratic José Beltrán Martínez, 2, 46980 Paterna, València, Spain

[‡]Institut für Anorganische und Analytsiche Chemie, Johannes-Gutenberg-Universität, Staudinger-Weg 9, D-55099 Mainz, Germany

[§]Department of Chemistry, Taras Shevchenko National University of Kyiv, Volodymyrska 64/13, 01601 Kyiv, Ukraine

Supporting Information

ABSTRACT: Surfactant-free nanocrystals of the model spin-crossover compound $[Fe(phen)_2(NCS)_2]$ (phen: 1,10-phenanthroline) have been synthesized applying the reverse micelle technique. The morphology of the nanocrystals, characterized by scanning electronic microscopy, corresponds to rhombohedric platelets with dimensions ranging from 203 × 203 × 106 nm to 142 × 142 × 74 nm. Variation of the concentration of the $Fe(BF_4)_2 \cdot 6H_2O$ salt in the synthesis has been found to have little influence on the crystallite size. In contrast, the solvent−surfactant ratio (ω) is critical for a good particle growth. The spin transition of the nanocrystals has been characterized by magnetic susceptibility measurements and Mössbauer spectroscopy. The nanocrystals undergo an abrupt and more cooperative spin transition in comparison with the bulk compound. The spin transition is centered in the interval of temperature of 175−185 K and is accompanied by 8 K of thermal hysteresis width. The crystallite quality more than the crystallite size is responsible for the higher cooperativity. The magnetic properties of the nanocrystals embedded in organic polymers such as polyethylene glycol, nujol, glycerol, and triton have been studied as well. The spin transition in the nanocrystals is affected by the polymer coating. The abrupt and first-order spin transition transforms into a more continuous spin transition as a result of the chemical pressure asserted by the organic polymers on the Fe(II) centers.

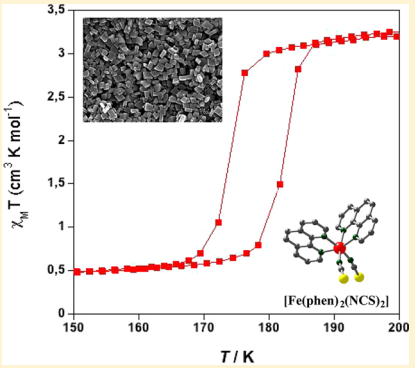

INTRODUCTION

Information storage in the contemporary society relies on an inherent property of the matter, electronic bistability. It refers to the ability of a system to be observed in two different electronic states of a certain range of some external perturbation: binary coding (0−1).[1] Molecular-based compounds offer an exciting opportunity to store information at nanometer scale, but silicon-based current technologies soon will reach the limit in size reduction. In addition, the response time of molecular devices can be in the range of femtoseconds whereas the fastest present devices operate at the nanosecond regime. The synthesis of bistable molecular compounds acting as processors of information is one of the most outstanding challenges of modern molecular chemistry and materials science. In relatively few years, the "naive" expectation of the use of a molecule to perform electronic functions has become a widespread research field, named "Molecular Electronics".[2]

One of the best examples of molecular electronic bistability is the spin-crossover (SCO) or spin-transition (ST) phenomenon.[3] It is known as the interconversion between the electronic spin states occurring in pseudo-octahedral coordination compounds of first transition series ions: chromium, manganese, iron, and cobalt with d^4, d^5, d^6, and d^7 electronic configurations. Of the ions that do show typical spin-crossover behavior, the largest number of examples is found for the iron(II). SCO compounds are switchable in a controlled, detectable, and reversible manner between two electronic states in thermodynamic competition: the low spin state (LS) and the high spin state (HS). In the HS and LS configurations, the compounds present distinct metal−donor atom distances (molecular volume), magnetic, dielectric, and optical (color) properties. Switching between the spin states can be induced by an external perturbation such as variation of temperature,[4] application of pressure,[5] or light irradiation.[6] Spin crossover compounds are potentially more useful than other magnetic molecules because their switching behavior can occur closer to room temperature, and they are thus prime candidates in Molecular Electronics and Spintronics for use in molecule-based devices.[2b]

The potential for technologic exploitation of SCO compounds was recognized in early 1990.[7] Since then, the

Received: April 30, 2015
Published: July 24, 2015

DOI: 10.1021/acs.inorgchem.5b00978
Inorg. Chem. 2015, 54, 7906−7914

Scheme 1. Schematic Illustration of the Processing of Spin-Crossover Materials at the Nanoscale

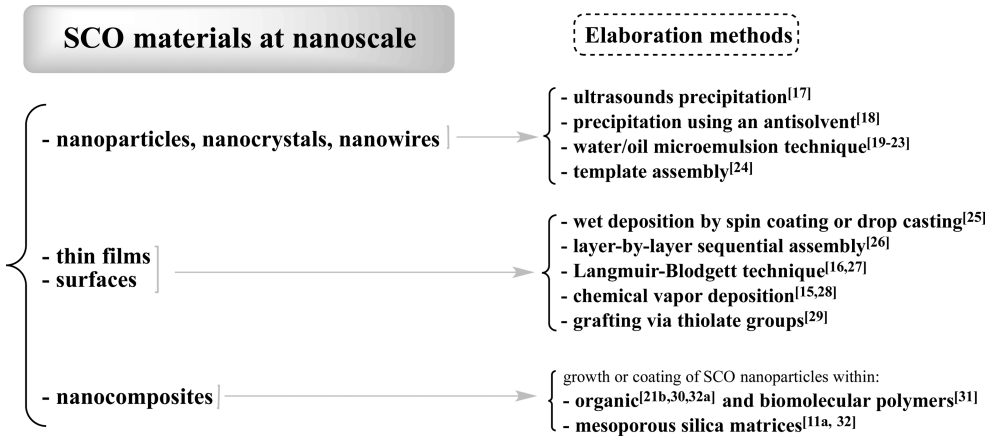

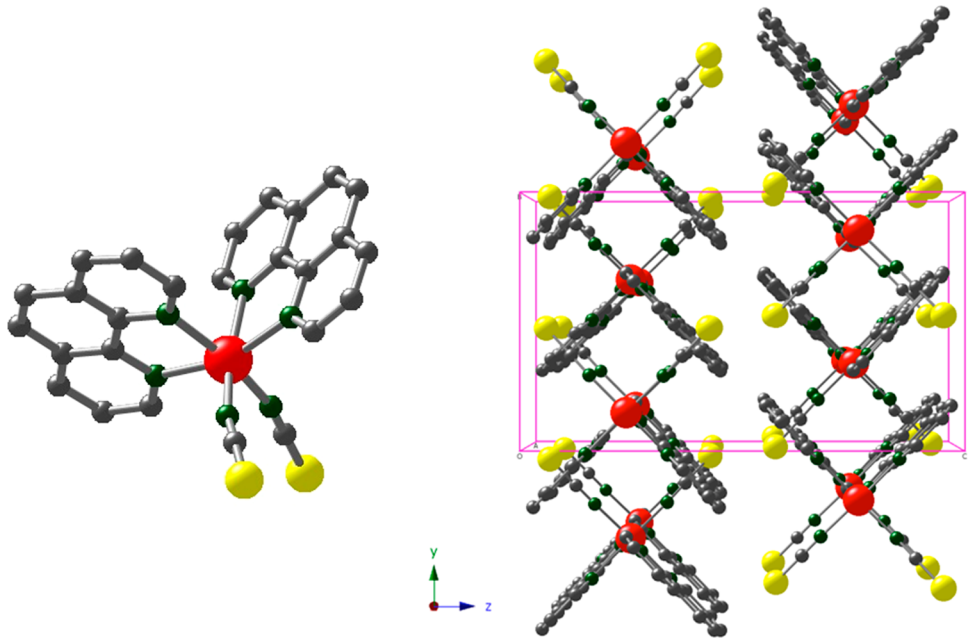

Figure 1. Illustration of the molecule $[Fe(phen)_2(NCS)_2]$ and its crystal packing in the *yz* plane (phen = 1,10-phenanthroline).

number of scientists interested in this research field as well as the number of papers and reviews published have increased considerably. Most of this work has been recently reviewed.[3a,b] Now that the stages of discovering and understanding of the fundamental aspects of SCO in the solid state and in solution have been overcome, the forefront research activities are focused essentially on the following:

(i) The synthesis of new molecule-based multifunctional materials in which the SCO properties may be combined with other physical or chemical properties in a synergetic fashion (i.e., *magnetic ordering,*[8] *electrical conductivity,*[9] *nonlinear optical response,*[10] *fluorescence,*[11] *and porous properties*).[12]

(ii) The study of SCO in "soft matter": *liquid crystals, gels, and dendrimers exhibiting spin-crossover properties.*[13]

(iii) The study of the SCO phenomenon at "nano scale": *nanoparticles, nanocomposites, thin films, and surfaces.*[14]

(iv) The study of the charge transport properties of single spin-crossover molecules.[15]

Investigation of the spin-crossover phenomenon at "nano scale" started less than one decade ago.[14] However, in the early 90s, the first thin films of Fe(II) SCO complexes prepared by employing the Langmuir−Blodgget technique were reported in the literature.[16] Scheme 1 shows a brief synopsis of the work done in this research topic until now. Nanoparticles, nanocrystals, nanowires, thin films, and nanocomposites have been obtained following different elaboration methods, and their spin-crossover properties have been studied.[17−32]

Compound $[Fe(phen)_2(NCS)_2]$[33] (phen: 1,10-phenanthroline) represents a model compound in the research field because it was the first Fe(II) complex synthesized that exhibited spin-crossover properties (Figure 1).[33a,b] $[Fe(phen)_2(NCS)_2]$ has become one of the most thoroughly studied and characterized spin-crossover systems, and it remains of current interest, even from a theoretical viewpoint. Such studies contributed to understand the SCO in solid state in great detail.[3] However, to the best of our knowledge, the synthesis of nanoparticles and the study of size-dependent spin-crossover properties have yet been not accomplished. Hereafter, we report the synthesis of nanocrystals of the [Fe-

DOI: 10.1021/acs.inorgchem.5b00978
Inorg. Chem. 2015, 54, 7906−7914

$(phen)_2(NCS)_2$] compound using the reverse micelle technique. The study of the spin-transition properties of the nanocrystals has been carried out by magnetic susceptibility measurements and the Mössbauer spectroscopy. Magnetic investigations of nanocrystals embedded in different organic polymers have been performed as well.

EXPERIMENTAL SECTION

Materials. $Fe(BF_4)_2{\cdot}6H_2O$ (97%), KSCN (98%) and 1,10-phenanthroline·H_2O (99%+) were obtained from Sigma-Aldrich. Sodium bis(2-ethylhexyl) sulfosuccinate NaAOT (96%) (CAS No. 577−11−7) and octane (97%) were obtained from Acros and used without further purification. The deionized water used for the synthesis was deoxygenated by simultaneous sonication and argon bubbling during 1 h. Polyethylenglycol, glycerol, triton, and nujol (technical grade) were obtained from Sigma-Aldrich.

Synthesis of Nanocrystals of [Fe(phen)$_2$(NCS)$_2$] (1−6). Two solutions containing 9.87 g (22.2 mmol) of NaAOT in 44 mL of octane were prepared in 250 mL dry spherical flasks. Initially, 33.75 mg (0.1 mmol) of $Fe(BF_4)_2{\cdot}6H_2O$ and 19.43 mg (0.2 mmol) of KNCS were dissolved in 2 mL of water and stirred for 2 min. The formed solution was slowly added to one of the flasks containing the NaAOT solution and stirred vigorously until formation of slightly yellowish water in oil (w/o) microemulsion. Similarly, a solution of 0.2 mmol (39.64 mg) of 1,10-phenanthroline·H_2O in 2 mL of methanol was slowly added to the second NaAOT solution under intensive stirring. The obtained w/o solutions (ω = [H_2O + MeOH]/[NaAOT] = 3.6, both concentrations related to the total volume of octane) were stirred for ∼15 min, then quickly combined in a flask previously purged with argon, and the resulting solution was left under vigorous stirring. Signs of precipitation appeared after ∼30 min of stirring. After 24 h of stirring, the precipitate was centrifuged at 3500 rpm during 30 min, yielding a purple precipitate and slightly red colored supernatant. The precipitate was washed via three cycles of redispersing in methanol and 15 min of centrifugation. The products were dried under air, yielding **1**−**6**. The yield of the fine precipitate in repeated experiments was about 50−60% for **1**−**6**. A flux diagram of the synthesis is provided in Figure S1. Anal. Calcd for $C_{26}H_{16}FeN_6S_2$ (**1**−**6**): C, 58.65; H, 3.03; N, 15.78. Found (**1**): C, 58.62; H, 3.01; N, 15.71; (**2**): C, 58.60; H, 3.02; N, 15.72; (**3**): C, 58.61; H, 3.01; N, 15.751; (**4**): C, 58.64; H, 3.02; N, 15.73; (**5**): C, 58.64; H, 3.03; N, 15.77; (**6**): C, 58.64; H, 3.02; N, 15.77. EDXA (energy-dispersive X-ray microanalysis) found: (30%Fe:70%S) **1**−**6**. Powder X-ray diffraction patterns were recorded for compounds **1**−**6** at 293 K and were found to match those corresponding to the bulk compound [Fe(phen)$_2$(NCS)$_2$] (Figure S2).

IR (Figure S3), characteristic bands in cm^{-1}: (**1**) 2061.4; 1513.1; 1424.3; 846.8; 724.9 (**2**) 2061.1; 1513.2; 1424.0; 846.3; 724.8 (**3**) 2061.2; 1513.1; 1424.1; 846.5; 724.9 (**4**) 2061.6; 1513.5; 1424.2; 846.4; 724.8 (**5**) 2061.2; 1513.1; 1424.1; 846.6; 724.9 (**6**) 2061.2; 1513.2; 1424.1; 846.5; 724.8.

Physical Characterization. Variable-temperature magnetic susceptibility measurements of all samples (10−15 mg) were recorded on a Quantum Design MPMS2 SQUID susceptometer equipped with a 5.5 T magnet, operating at 1 T and in the 1.8−400 K temperature interval. Experimental susceptibilities were corrected for diamagnetism of the constituent atoms using Pascal's constants.[1b] Mössbauer spectra were recorded in transmission geometry with a ^{57}Co/Rh source kept at room temperature and a conventional spectrometer operating in the constant-acceleration mode. The samples were sealed in acrylic sample holders and mounted in a nitrogen bath cryostat. The Recoil 1.05 Mössbauer Analysis Software (Dr. E. Lagarec; http://www.isapps.ca/recoil/) was used to fit the experimental spectra. SEM analysis was performed on a HITACHI S-4800 microscope. The software used for processing of images was "ImageJ".[34] IR spectra were recorded at 293 K in KBr using a Nicolet 5700 FTIR spectrometer. The equipment used for PXRD characterization of compounds was a Seifert XRD 3003 TT diffractometer, with Bragg−Brentano geometry and Cu tube working at 40 kV with Ni filter (0.3 mm primary slit, 0.3 mm secondary slit, 0.2 mm detector slit and scintillation detector).

RESULTS

Experimental Conditions for Nanocrystals Growth and Their Optimization. Nanocrystals of [Fe(phen)$_2$(NCS)$_2$] were obtained applying the reverse micelle method.[35] The syntheses were done at room temperature by mixing NaAOT stabilized water in oil (w/o) microemulsions containing $Fe(BF_4)_2{\cdot}6H_2O$, KNCS, and 1,10-phenanthroline at a fixed ω = [solvent]/[NaAOT] ratio. The first experiments were performed at ω = 5 with [Fe^{II}] = 0.1 M and different reaction times, 1, 2, 4, and 24 h. A few minutes after mixing of the colorless solutions, a distinctive color change to intense red-violet was observed. A fine precipitate constituted of nanocrystals appeared within 30 min. The nanocrystals' growth takes place via content exchange between microdroplets of the microemulsions, and their precipitation occurs at some particle size limit, apparently, because of destabilization of the micelle. The yield was very low at reaction times equal to 1, 2, and 4 h, in which only 1 mg of compound was isolated. In contrast, the yield increased up to 10−20 mg when the reaction time was 24 h. The samples have been characterized by scanning electron microscopy (SEM) (see Table S1a). From the images, one can infer that the crystallization process was not finished when the reaction was stopped—the particles are not regular. The morphology of the particles can be envisaged as rhombohedric. Subsequent syntheses were done by varying the [solvent]/[NaAOT] ratio and the concentration around this initial point with the purpose of achieving different optima regarding the size and shape of the nanocrystals. The concentration was increased up to 0.15 and 0.2 M, maintaining ω = 5 and the reaction time of 24 h. The regularity of the nanocrystals was not improved at [Fe^{II}] = 0.2 M, but the yield increased considerably (60 mg). Satisfactory results were obtained decreasing the ω ratio, particularly at ω = 3.6. Several experiments were performed at this ω varying the concentration of [Fe^{II}], 0.1, 0.15, 0.2, 0.3, 0.4, and 0.5 M, while keeping the reaction time at 24 h (Table 1). Regular rhombohedric crystals of nanometric size were obtained in all cases (samples **1**−**6**). Reproducibility of the syntheses was proven several times (see Supporting Information (SI)). Particles of compound [Fe(phen)$_2$(NCS)$_2$] did not form at ω = 3.6 and [Fe^{II}] = 0.05 M or lower ω ratios, independently of the reaction time. Instead, red solutions containing the compound {[Fe(phen)$_3$](NCS)$_2$} were obtained.

Given that the attempts to synthesize smaller nanocrystals using the reverse micelle method were unsuccessful, we decided to explore the formation of nanoparticles/nanocrystals using polyvinylpyrrolidone (PVP) as a protecting polymer. However, this approach lead to agglomerates of crystals of micron dimensions with different morphology, hexagonal and prismatic platelets (Table S1b).

Particle Size Determination from Scanning Electron Microscopy Images (SEM) (1−6, 1* and 2*). Figure 2 contains a selection of images of samples **1**−**6** obtained with SEM. As anticipated above, the morphology of the nanocrystals is rhombohedric in all samples. The average particle sizes found and distribution are compiled in Table 1 and SI (Table S2). For statistical estimations of the rhombohedron's dimensions, L and W (length and width), at least ∼200 particles were evaluated for each sample. SEM analysis pointed out that the concentration of reactants does not have a strong influence in

DOI: 10.1021/acs.inorgchem.5b00978
Inorg. Chem. 2015, 54, 7906−7914

Table 1. Synthetic Conditions, Morphology of the Crystals, Dimensions, Average Particle Size Distribution, Standard Deviation, and Critical Temperatures of the Spin Transition for Samples 1−6[a]

sample code	[Fe(II)] mmol	ϖ = [solvent]/ [NaOT]	reaction time (h)	temperature (K)	morphology	$a \times b \times c$ $(nm)^3$	L (length) (nm)	W (width) (nm)	$T_c\downarrow$(K)	$T_c\uparrow$(K)	ΔT_c (K)
1	0.1	3.6	24	293	rhombohedric	203 × 203 × 106	203 ± 38	106 ± 17	174.2	182.5	8.3
2	0.15	3.6	24	293	rhombohedric	162 x162 × 79	162 ± 22	79 ± 11	174	182.5	8.5
3	0.2	3.6	24	293	rhombohedric	171 x171 × 85	171 ± 26	85 ± 12	175.1	182.2	7.1
4	0.3	3.6	24	293	rhombohedric	142 x142 × 74	142 ± 23	74 ± 13	177.2	183.3	6.1
5	0.4	3.6	24	293	rhombohedric	158 × 158 × 76	158 ± 22	76 ± 13	175	183.3	8.3
6	0.5	3.6	24	293	rhombohedric	163 × 163 × 80	163 ± 28	80 ± 13	177.5	184.2	6.7

[a]The nanocrystals have been obtained using the reverse micelle technique.

determining the particle size. For the experiment with the smaller concentration of Fe^{II} (0.1 M), the biggest particles have been obtained, 203 × 203 × 106 nm. As the concentration of Fe^{II} increases, the particle dimensions slightly decrease. However, similar particle dimensions have been found for the experiments with $[Fe^{II}]$ = 0.15 and 0.5 M, 162 × 162 × 79 and 163 × 163 × 80 nm, respectively. The particle size distribution has been found very narrow for all samples and for both dimensions, L and W. In fact, for samples **2**−**6**, the standard deviation for the dimension L ranges from 22 to 28 nm, whereas for the dimension W, it is between 11 and 13 nm. For sample **1**, the standard deviation is a bit larger, 38 nm (L) and 17 nm (W).

In order to prove the reproducibility of the synthesis of nanocrystals, the experiments have been repeated several times for each Fe^{II} concentration. In particular, the synthesis has been reproduced 10 times for $[Fe^{II}]$ = 0.1 and 0.15 M. The morphology has been found identical and the particle dimensions very similar in each series of experiments of samples **1**−**6** (see SI). Interestingly, when reproducing the synthesis of **1** [$[Fe^{II}]$ = 0.1] and **2** [$[Fe^{II}]$ = 0.15], among a series of 10 experiments, we found nanocrystalline samples with defects (small holes) on the surface (Table S3, Figure S2). These samples have been labeled as **1*** and **2***. The morphology of the nanocrystals as well as the dimensions of **1** and **1*** are practically identical. They are rhombohedric platelets, whose dimensions are 203 × 203 × 106 nm (**1**) and 206 × 206 × 106 nm (**1***). The standard deviation of L and W dimensions for **1** and **1*** is very close [L: 38(**1**) and 40(**1***) nm; W: 17(**1**) and 19(**1***) nm]. The same accounts for samples **2** and **2***, but the nanocrystal's dimensions are slightly larger for **2*** [194 × 194 × 94 nm (**2***); 162 × 162 × 79 nm (**2**)] [L: 24(**2***) and 22(**2**) nm; W: 12(**2***) and 11(**2**) nm]. The magnetic properties of samples **1** and **2** differ from those of **1*** and **2*** in the thermal hysteresis width associated with the spin transition (*vide infra*).

Mössbauer Spectroscopy Characterization of the Nanocrystals (1 and 1*). The ^{57}Fe Mössbauer spectra of nanocrystals **1** measured at two representative temperatures are shown in Figure 3. High-temperature Mössbauer spectra for **1** show only one doublet characterized by isomer shift (δ, relative to α-iron) and quadrupole splitting (ΔE_Q) of 0.982(3) mms^{-1} and 2.652(6) mms^{-1}, respectively, which corresponds to the HS state. After being cooled to 84 K, all the HS sites have transformed into the LS sites. At 84 K, δ and ΔE_Q for the LS state deduced from the least-squares-fit routine analysis of the spectrum are, 0.465(2) mms^{-1} and 0.360(3) mms^{-1}, respectively. The line width for the HS and LS states is Γ(HS) = 0.136(4) mm/s and Γ(LS) = 0.144(2) mm/s. The characteristic Mössbauer parameters, δ and ΔE_Q, of the nanocrystals match with those reported for the [Fe(phen)$_2$(NCS)$_2$] bulk compound.[36]

The Mössbauer spectra of sample **1*** at 293 and 84 K are given in Figure S5. The doublets and the parameters δ and ΔE_Q of **1*** at high and low temperature are very similar to those observed for **1**. The low-temperature spectrum evidences a complete transformation of the Fe^{II} centers to the LS state.

Magnetic Properties of the Nanocrystals (1−6, 1*, and 2*). Figure 4 gathers the thermal dependence of $\chi_M T$ for samples **1**−**6**, where χ_M stands for the molar magnetic susceptibility and T for temperature. The measurements have been performed at the rate of 2 K/min in the cooling and warming modes. At 200 K, the $\chi_M T$ value for samples **1**−**6** was

DOI: 10.1021/acs.inorgchem.5b00978
Inorg. Chem. 2015, 54, 7906−7914

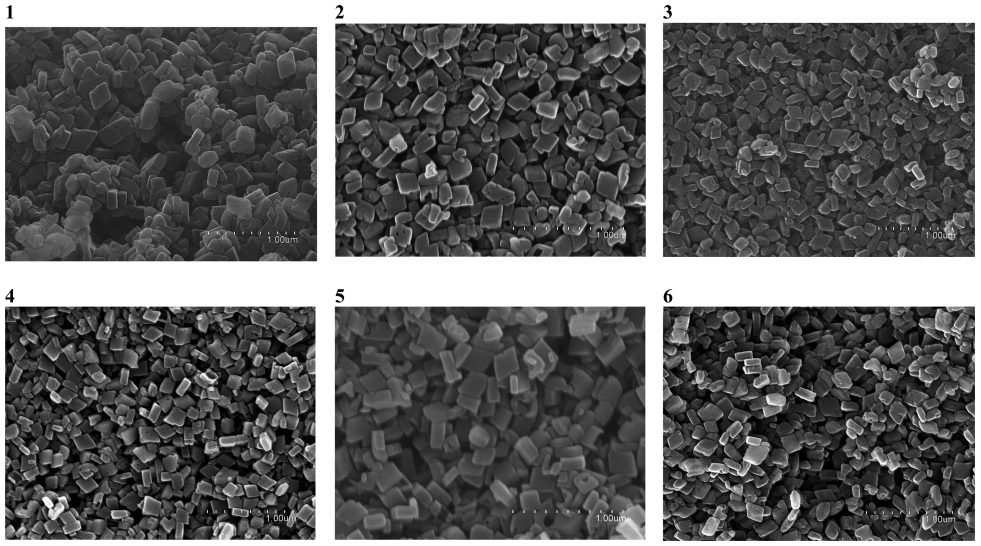

Figure 2. Image of the nanocrystals **1**−**6** obtained with the scanning electronic microscope (SEM).

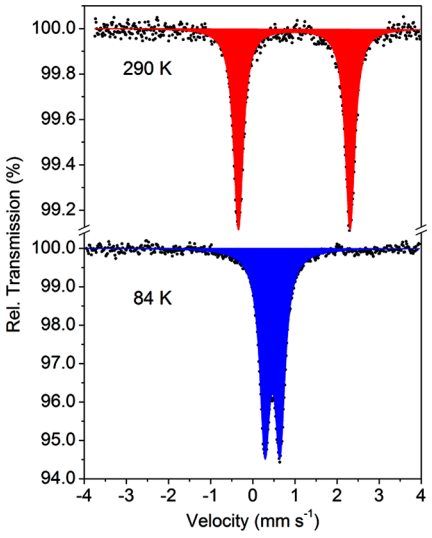

Figure 3. Mössbauer spectra of **1** measured at 290 and 84 K (blue: LS doublet; red: HS doublet).

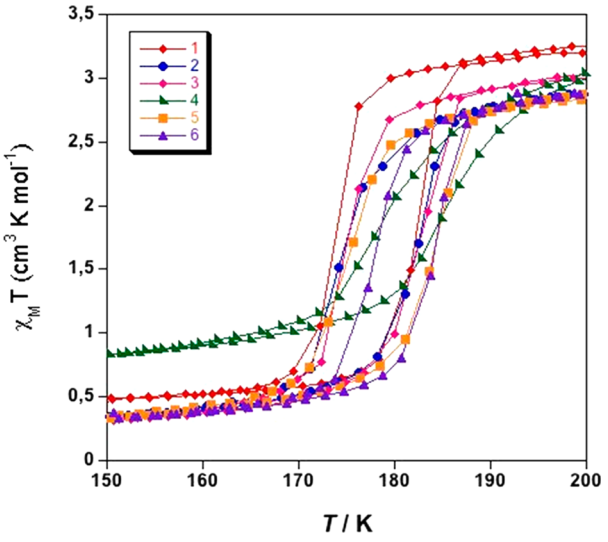

Figure 4. Magnetic properties of the nanocrystals **1**−**6** in the form of $\chi_M T$ vs T, where χ_M is the molar magnetic susceptibility and T is the temperature.

found in the range 3.20−2.90 cm^3 K mol^{-1}. For sample **1**, the Mössbauer spectrum measured at 290 K denoted that all Fe^{II} centers were in the HS state. If any, the LS fraction for **1** at high temperature has to be less than 2%, which is the detection limit of the technique. Therefore, the $\chi_M T$ values found below 3.20 cm^3 K mol^{-1} indicate the presence of a small LS residual fraction, less than 9%. On cooling, $\chi_M T$ diminishes abruptly as a consequence of the spin transition occurring in samples **1**−**6**. The critical temperatures of the spin transition, T_c, regarded as a first order spin transition, are listed in Table 1. For all samples, the critical temperature in the cooling mode, $T_c\downarrow$, is located between 174 and 177 K, whereas $T_c\uparrow$ (warming mode) is in the interval of 182−184 K, giving thermal hysteresis loops of 6 or 8 K (ΔT_c). Below and above, $T_c\downarrow$ and $T_c\uparrow$, respectively, the magnetic susceptibility is temperature-independent. At 20 K, samples **1**−**6** exhibit $\chi_M T$ values of 0.10−0.15 cm^3 K mol^{-1}. This residual paramagnetism may be due to the presence of a very small HS residual fraction (<3%) or could be associated with the temperature-independent paramagnetism (TIP)[1] of the Fe^{II} ions as well. Both HS and LS residual fractions originate from crystal lattice defects as it is well documented for spin-crossover complexes.

The magnetic properties of nanocrystals **1*** and **2*** are depicted together with those of **1** and **2** in Figure 5. The thermal hysteresis observed in sample **1** is 3 times larger than that observed for **1*** [ΔT_c (K): 8.3(**1**) and 3(**1***)]. The critical temperatures for sample **1*** have been found to be, $T_c\downarrow$ and $T_c\uparrow$, 180.4 and 183.4 K, respectively, and the $\chi_M T$ value at 20 and 200 K, identical to those for **1** (0.10 and 3.20 cm^3 K mol^{-1}). The $T_c\downarrow$ and $T_c\uparrow$ are 181 and 182 K for **2*** [ΔT_c(K): 1(**2***)]. In comparison, the ΔT_c for **2** is much larger, 8.5 K.

The magnetic properties of the bulk compound [Fe(phen)$_2$(NCS)$_2$] have been studied extensively.[33a,b,d,k] The spin-transition characteristics, particularly, sharpness, thermal hysteresis, and residual high spin fraction at low temperature depend in large extent to the synthetic method employed. The "precipitated" and "crystallized"[33d,f] samples undergo spin transition at T_c = 176 K with no more than 1 K of hysteresis width and a HS residual fraction of 17%. In contrast, the

DOI: 10.1021/acs.inorgchem.5b00978
Inorg. Chem. 2015, 54, 7906−7914

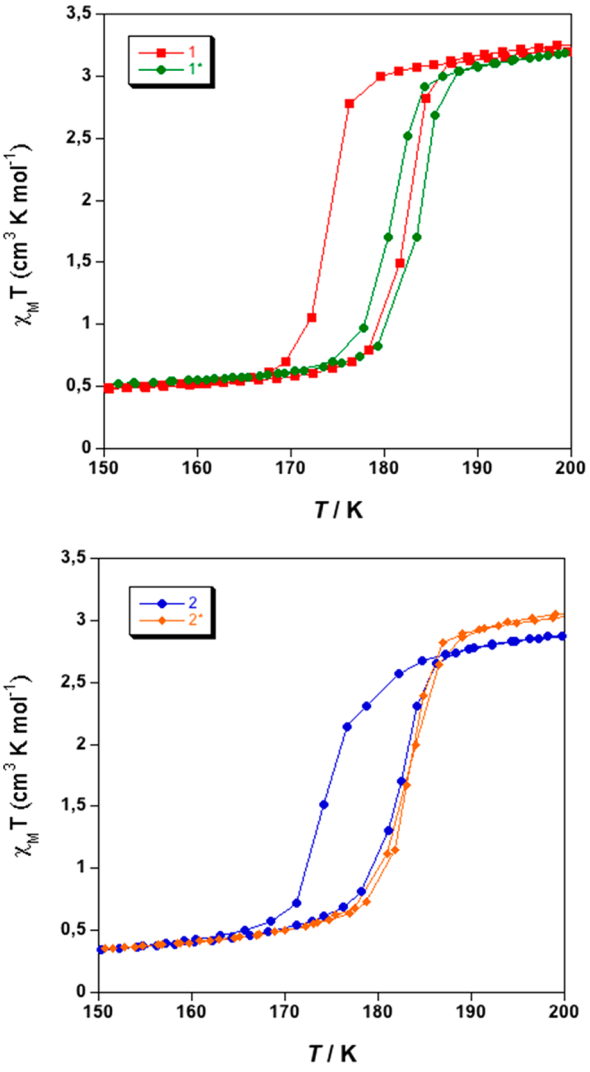

Figure 5. Magnetic properties of the nanocrystals **1**−**1*** and **2**−**2*** in the form of $\chi_M T$ vs T.

"extracted" sample shows more abrupt and complete spin transition centered at 176 K with ΔT_c equal to 0.15 K.[33b] The discrepancies in the magnetic behavior have been ascribed to differences in size and quality of the crystallites because powder X-ray diffraction and IR studies have not shown any differences among samples. The nanocrystals **1**−**6** undergo more cooperative spin transition in comparison with the bulk compound. The wider thermal hysteresis width associate with the spin transitions illustrates it.

Magnetic Properties of the Nanocrystals (3) Dispersed in Organic Polymers. The magnetic properties of the nanocrystals of sample **3** dispersed in four liquid organic polymers of different chemical composition and density, including polyethylene glycol (PEG), nujol, glycerol, and triton, have been investigated (Figure 6). At 293 K, the density of the polymers expressed in g/mL is as follows: PEG (1.13), nujol (0.838), glycerol (1.26), and triton (1.07). Around 15 mg of **3** were placed in a sample holder filled each time with one polymer. The nanocrystals were dispersed inside the liquid polymers making use of a glass stick. Homogeneous suspensions of **3** in polymers were achieved. The sample holder was cooled quickly to 50 K and subsequently to 20 K in order to frozen the suspensions. The temperature dependence

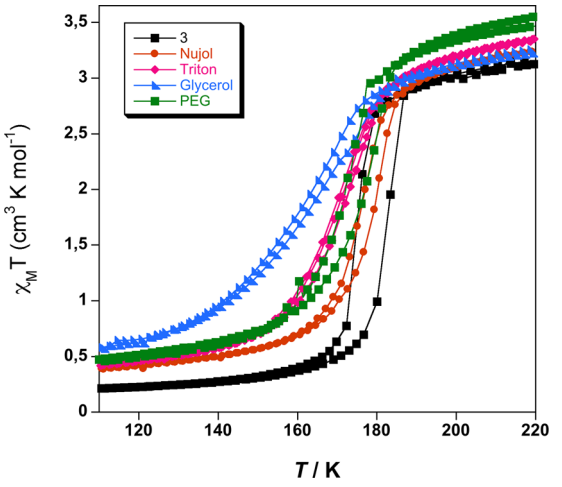

Figure 6. Magnetic properties of the nanocrystals **3** embedded in polymers: polyethylene glycol (PEG), nujol, glycerol, triton.

of the magnetic susceptibility was then measured following the sequence 20 K- 300 K- 20 K.

The nanocrystals **3** experience a remarkable change of the magnetic properties when they are dispersed in the polymers (Figure 6). At 210 K, the $\chi_M T$ value of **3** is slightly different, PEG (3.48), nujol (3.18), glycerol (3.16), and triton (3.29) cm^3 $K\ mol^{-1}$, but almost all Fe^{II} centers are in the HS configuration. Embedded in polymers, **3** exhibit more continuous spin transition, and the characteristic temperatures are shifted downward (Table 2). The thermal hysteresis associated with

Table 2. Critical Temperatures of the Spin Transition for Samples 3 Dispersed Organic Polymers

3 dispersed in:	$T_c\downarrow$(K)	$T_c\uparrow$(K)	ΔT_c (K)
PEG	170	175	5
nujol	175	179	4
glycerol	160	162	2
triton	170	172	2
3	175.1	182.2	7.1

the spin transition becomes narrower as well. Indeed, ΔT_c diminished to 5 and 4 K, in the case of PEG and nujol, respectively, whereas it is 2 K for glycerol and triton. Below $T_c\downarrow$, the magnetic susceptibility is practically temperature independent, and its value of 0.5−0.2 cm^3 $K\ mol^{-1}$ indicates that practically all the Fe^{II} centers are in the LS state.

Powder X-ray Diffraction of Nanocrystals (1−6, 1*, and 2*). The powder X-ray diffraction pattern (XRPD) of nanocrystals **1**−**6**, **1***, and **2*** collected at 293 K match the simulated one for the HS structure of $[Fe(phen)_2(NCS)_2]$[33d,f] at the same temperature (Figure S3). Nanocrystals **1**−**6**, **1***, and **2*** have very similar profiles, where the representative peaks are as follow: $2\theta(hkl)$: 10.11°(002); 10.98°(110); 12.10°(111); 13.44°(200); 14.94°(112); 16.81°(211); 17.43°(020); 23.20°(023); 26.88°(024); 27.74(124); 34.14(134); 41.41(136).

Integral width (β_{hkl}) values for the 110, 111, 002, and 023 reflections were used to determine the particle size based on Scherrer's eq (Table S3). Figure S6 gathers a comparative analyses of the particle size deduced applying the Scherrer equation and from SEM measurements. Both estimations denote the correlation between the crystallite size and the Fe^{II}

DOI: 10.1021/acs.inorgchem.5b00978
Inorg. Chem. 2015, 54, 7906−7914

concentration. The crystallite size diminishes as the concentration increases. SEM analysis determines that sample **4** presents the smallest dimension ($142 \times 142 \times 74$ nm^3), and this result agrees with the Scherrer estimation, because the largest value of (β_{obs}) corresponds to sample **4**.

IR Spectra of (1−6, 1*, and 2*). Figure S4 gathers the IR spectra of nanocrystals measured at 293 K (HS state). The absence of significant surfactant amounts covering the nanocrystals is proved by the lack of any characteristic IR absorption band (see for instance the IR spectra of the sodium bis(2-ethylhexyl) sulfosuccinate given in the SI).

The characteristic IR bands for the bulk compound $[Fe(phen)_2(NCS)_2]$ appears in the interval of 1650−600 cm^{-1} together with the band corresponding to NC(S) stretching mode at 2061 cm^{-1}.[37] The spectra are slightly different for the compound in the HS and LS state. Among all found bands, which are sensitive to the electronic configuration of the metal, there is at least one reliable spectral marker. It is the band of CC, CN stretchings at ∼1500 cm^{-1}, which grows essentially relative to the complex feature at ∼1580 cm^{-1} with population of high-lying 3d-orbitals of metal centers. The changes of IR intensities during LS−HS transition are mainly caused by electron density transfer from metal to ligands. For the HS state, the most characteristic bands are as follows. The band related to NC(S) stretching modes locates at 2061 cm^{-1}, while those corresponding to the phenathroline ring appear at the following: 1515 and 1495 cm^{-1} (C−C and C−N stretching vibrations); 867 and 728 cm^{-1} (C−H out of plane bending modes); 1100 and 640 cm^{-1} (C−H in plane bending modes). The IR bands found for nanocrystals **1**−**6**, **1***, and **2*** match well those reported in the literature for $[Fe(phen)_2(NCS)_2]$ in the HS state.

DISCUSSION

As stated in the Introduction, the nanostructuration using the bottom-up synthetic approach is one of the forefront research activities in the field. Bistability depends on the collective behavior of the SCO centers in the lattice. Therefore, determining the critical film thickness or particle size necessary to preserve the first-order spin transition in SCO materials is imperative.

The majority of studies at nanoscale have been focused on Fe^{II} SCO complexes that exhibit very cooperative spin transitions centered close or at room temperature. Few are devoted to Fe^{III} SCO complexes.[24,25c] The most numerous studies on Fe^{II} complexes concern the one-dimensional triazole based polymers, $[Fe(R\text{-}trz)_3]X_2$ (R-trz: 4-susbtituted-1,2,4-triazole, X: anions)[17,18c,22a,c,23,27,25a,b,27b,30,32b,c] or $[Fe(Htrz)_2(trz)](BF_4)$[19] because they are very robust materials, easy and cheap to synthesize, and exhibit a very noticeable change of color upon spin transition at room temperature (from purple (LS) to white (HS)). The spin transition in nanoparticles of compounds $[Fe(NH_2\text{-}trz)_3]X_2$ have been found to be size-dependent, while in $[Fe(Htrz)_2(trz)](BF_4)$, the bistability does not depend on the particle size. For compounds $[Fe(R\text{-}trz)_3]X_2$, the critical temperature of the spin transition is shifted down in temperature as the particle size diminishes and the hysteresis width vanishes at a critical particle size. By contrast, small particles ∼10 nm of $[Fe(Htrz)_2(trz)](BF_4)$ show a complete and abrupt first-order spin transition. In both cases, the particle morphology, spherical or rectangular prism, apparently does not play a major role in determining the spin-transition characteristics. A concise correlation study between the film thickness and the critical temperatures of the spin transition has yet been not performed on these polymers.[25a−e,27b] The other types of materials widely investigated are cyanide-based spin-crossover two-dimensional and three-dimensional polymers of formulas $[Fe(L)_xM(CN)_4]$ (x = 1 or 2, L: pyrazine, pyridine, or bis-pyridine, M(II): Ni, Pd and Pt).[20,21,26,31] They undergo abrupt spin transitions located at room temperature or in the interval of 220−280 K accompanied by 25−40 K of thermal hysteresis width. The change of color is very noticeable as well, from red (LS) to yellow (HS). The nanocrystals/nanoparticles have shown a strong correlation between the magnetic properties and the crystallite size. The T_c values displace to low temperatures as particle size decreases and the thermal hysteresis diminishes. Residual HS and LS fractions appear as a consequence of the particle diminution. These effects are directly connected with the "chemical pressure" felt by the spin-transition centers, which diminishes as particle dimensions decrease.[20,21,31] By contrast, the spin-transition characteristics in thin films of these polymers are very comparable to those exhibited by the bulk complexes.[26]

Regarding studies of complex $[Fe(phen)_2(NCS)_2]$ at nanoscale, it is worth mentioning the synthesis of thin films obtained under vacuum sublimation[28a] and by drop casting[25f] performed very recently. Homogeneous films of $[Fe(phen)_2(NCS)_2]$ were obtained by thermal evaporation under vacuum, whereas lines of crystallites were obtained by drop casting. The spin transition in the homogneous films was found very comparable to the bulk compound, as well as for the nanostripes of crystallites.[25f]

The main conclusion learned in the present study is that the cooperativity associate with the spin transition in $[Fe(phen)_2(NCS)_2]$ strongly depends on the quality of the crystals—presence of crystals defects—not on the particle size, at least within the range of particle's size studied. Indeed, the thermal hysteresis width is very much influenced by the crystal defects. Precedent studies pointed at the particle size and crystal defects as responsible for the differences in spin-transition behavior found for precipitated, crystallized, and extracted samples of $[Fe(phen)_2(NCS)_2]$.[33b,d,f] **1*** and **2*** present very similar crystallite dimensions than observed for **1** and **2**. However, the SEM photographs obtained for **1*** and **2*** (Figure S2) denote the presence of an important number of defects seen as small holes. Seemingly, these crystal defects are responsible for the less cooperative spin transition observed for **1*** and **2*** in comparison with **1** and **2**, respectively. The thermal hysteresis width is four times larger in the case of **1** and **2**. A fact that additionally supports this statement is that the spin transition is not very much affected when the dimensions W and L of the crystallites diminish, as it is observed for samples **1**−**6**. The spin transition and hysteresis width is very similar for all samples. These results point at that the critical "crystal size" necessary to observe a first-order spin transition in $[Fe(phen)_2(NCS)_2]$ is below $142 \times 142 \times 74$ nm.

The effect of polymer coating on spin-crossover nanoparticles has already been investigated for complexes $[Fe(pz)Pt(CN)_4]$[32a] and $[Fe(3\text{-}F\text{-}py)_2M(CN)_4]$.[21b] A second-order spin transition has been observed for covered nanoparticles with noticeable HS and LS residual fractions at low and high temperature. The covering of nanocrystals by organic polymers produce an additional chemical pressure on the Fe(II) sites that leads to crystal defects and stabilization of the LS state. For particles of the $[Fe(phen)_2(NCS)_2]$ compound of micron

DOI: 10.1021/acs.inorgchem.5b00978
Inorg. Chem. 2015, 54, 7906−7914

dimensions, such types of studies have been performed recently as well.[38] The abrupt spin transition observed for the bulk compound transforms into more continuous and asymmetric spin transition when dispersed in solid matrices of the organic polymers. One noticeable fact is that depending on the elasticity of the polymer used, the 1 K hysteresis width (bulk) spans to 8−10 K. These effects are explained on the basis of chemical pressure imposed by the organic polymers, which is analogous to the effect of hydrostatic pressure on spin-crossover complexes.[5] In case of $[Fe(phen)_2(NCS)_2]$ nanocrystals, a transformation of the first-order spin transition into a second-order continuous spin transition is observed when they are dispersed in organic polymers.

CONCLUSION

Rhombohedric nanocrystals of dimensions ∼200 × 200 × 100 nm of the model spin-crossover complex $[Fe(phen)_2(NCS)_2]$ have been synthesized applying the reverse micelle technique. In contrast to the bulk compound, the nanocrystals undergo more cooperative first-order spin transition exhibiting a thermal hysteresis of ∼8 K. The crystallite quality more than the crystallite size is responsible for the higher cooperativity. The coating of the nanocrystals with organic polymers evidenced a transformation from the first-order spin transition to a more continuous second-order spin transition.

ASSOCIATED CONTENT

Supporting Information

Scheme of the synthesis of nanocrystals of compound $[Fe(phen)_2(NCS)_2]$, series of experiments performed in the synthesis of nanocrystals of compound $[Fe(phen)_2(NCS)_2]$ applying the reverse micelle method and using PVP as coating polymer, images used for particle size determination and the resultant statistics for the samples **1**−**6**, SEM photographs illustrating the crystal defects in samples **1*** and **2***, powder X-ray diffraction patterns of $[Fe(phen)_2(NCS)_2]$ at 293 K: calculated from the crystal structure and the nanocrystals **1**−**6** (experimental), IR spectra recorded at 293 K for **1**−**6**, **1***, and **2*** and for sodium bis(2-ethylhexyl) sulfosuccinate (NaOT), Mössbauer spectra of **1*** measured at 293 and 84 K. Summary on crystallite sizes for **1**−**6** obtained from Scherrer's equation using the reflections (002), (110), (111), and (023). Comparison of the crystallite's size obtained from SEM measurements and from Scherrer equation for samples **1**−**6**. The Supporting Information is available free of charge on the ACS Publications website at DOI: 10.1021/acs.inorgchem.5b00978.

AUTHOR INFORMATION

Corresponding Authors

*E-mail: ana.b.gaspar@uv.es.

*E-mail: jose.a.real@uv.es.

Notes

The authors declare no competing financial interest.

ACKNOWLEDGMENTS

This work was supported by the Spanish Ministerio de Ciencia e Innovación (MICINN) (presently Ministerio de Economía y Competitividad) and FEDER funds (CTQ2013-46275-P), the Generalitat Valenciana through PROMETEO/2012/049. F.J.V.-M. thanks the PROMETEO project for a predoctoral fellowship. A.B.G. acknowledges the Alexander von Humboldt foundation for working-visit fellowships. We thank Mr. Johannes Weihermüller from the University of Bayreuth (Germany) (Erasmus student, Valencia 2014) for his assistance in the synthesis of the nanocrystals.

REFERENCES

(1) (a) Verdaguer, M.; Robert, V. In *Comprehensive Inorganic Chemistry II: From Elements to Applications*; Reedijk, J., Poeppelmeier, M., Eds.; Elsevier: Amsterdam, 2013; Vol. *8*, pp 131−189. (b) Kahn, O. *Molecular Magnetism*; VCH: Weinheim, 1993.

(2) (a) Ratner, M. *Nat. Nanotechnol.* **2013**, *8*, 378−381. (b) Aradhya, S. V.; Venkataraman, L. *Nat. Nanotechnol.* **2013**, *8*, 399−410.

(3) (a) Gütlich, P.; Gaspar, A. B.; García, Y. *Beilstein J. Org. Chem.* **2013**, *9*, 342−391. (b) Gütlich, P. *Eur. J. Inorg. Chem.* **2013**, *2013*, 581−591. (c) Muñoz, M. C.; Real, J. A. *Coord. Chem. Rev.* **2011**, *255*, 2068−2093. (d) Bousseksou, A.; Molnár, G.; Salmon, L.; Nicolazzi, W. *Chem. Soc. Rev.* **2011**, *40*, 3313−3335. (e) Halcrow, M. A. *Chem. Soc. Rev.* **2011**, *40*, 4119−4142. (f) Sorai, M.; Nakazawa, Y.; Nakano, M.; Miyazaki, Y. *Chem. Rev.* **2012**, *113*, PR41−PR122. (g) Real, J. A.; Gaspar, A. B.; Muñoz, M. C. *Dalton Trans.* **2005**, 2062−2079. (h) *Spin Crossover in Transition Metal Compounds I−III, Topics in Current Chemistry*; Gütlich, P., Goodwin, H. A., Eds.; Springer-Verlag: Berlin, 2004; Vols. *233*−*235*. (i) *Spin-Crossover Materials: Properties and Applications*; Halcrow, M. A., Ed.; John Wiley & Sons Ltd.: Chichester, 2013. (j) *European Journal of Inorganic Chemistry Special Issue: Spin-Crossover Complexes (Cluster Issue)*, Issue 5−6; Murray, K. S., Real, J. A., Oshio, H., Eds; Wiley-VCH.: Weinheim, 2013.

(4) Gütlich, P.; Goodwin, H. A. *Top. Curr. Chem.* **2004**, *233*, 1−47.

(5) Gütlich, P.; Ksenofontov, V.; Gaspar, A. B. *Coord. Chem. Rev.* **2005**, *249*, 1811−1829.

(6) (a) Hauser, A. *Top. Curr. Chem.* **2004**, *234*, 155−198. (b) Lètard, J. F. *J. Mater. Chem.* **2006**, *16*, 2550−2559.

(7) (a) Kahn, O.; Kröber, C.; Jay, C. *Adv. Mater.* **1992**, *4*, 718−728. (b) Kahn, O.; Martinez, J. *Science* **1998**, *279*, 44−48. (c) Lètard, J. F.; Guionneau, P.; Goux-Capes, L. *Top. Curr. Chem.* **2004**, *235*, 221−249. (d) Galet, A.; Gaspar, A. B.; Muñoz, M. C.; Bukin, G. V.; Levchenko, G.; Real, J. A. *Adv. Mater.* **2005**, *17*, 2949−2953.

(8) (a) Ohkoshi, S. I.; Tokoro, H. *Acc. Chem. Res.* **2012**, *45*, 1749−1758. (b) Gaspar, A. B.; Muñoz, M. C.; Real, J. A. *J. Mater. Chem.* **2006**, *16*, 2522−2533.

(9) (a) Takahashi, K.; Cui, H. B.; Okano, Y.; Kobayashi, H.; Mori, H.; Tajima, H.; Einaga, Y.; Sato, O. *J. Am. Chem. Soc.* **2008**, *130*, 6688−6689. (b) Xue, W.; Wang, B. Y.; Zhu, J.; Zhang, W. X.; Zhang, Y. B.; Zhao, H. X.; Chen, X. M. *Chem. Commun.* **2011**, *47*, 10233−10235.

(10) Bonhommeau, S.; Lacroix, P. G.; Talaga, D.; Bousseksou, A.; Seredyuk, M.; Fritsky, I. O.; Rodriguez, V. *J. Phys. Chem. C* **2013**, *116*, 11251−11255.

(11) (a) Titos-Padilla, S.; Herrera, J. M.; Chen, X. W.; Delgado, J. J.; Colacio, E. *Angew. Chem., Int. Ed.* **2011**, *50*, 3290−3293. (b) Salmon, L.; Mòlnar, G.; Zitouni, D.; Quintero, C.; Bergaud, C.; Micheau, J. C.; Bousseksou, A. *J. Mater. Chem.* **2010**, *20*, 5499−5503.

(12) (a) Ohba, M.; Yoneda, K.; Agustí, G.; Muñoz, M. C.; Gaspar, A. B.; Real, J. A.; Yamasaki, M.; Ando, H.; Nakao, Y.; Sakaki, S.; Kitagawa, S. *Angew. Chem., Int. Ed.* **2009**, *48*, 4767−4771. (b) Southon, P. D.; Liu, L.; Fellows, E. A.; Price, D. J.; Halder, G. J.; Chapman, K. W.; Moubaraki, B.; Murray, K. S.; Lètard, J. F.; Kepert, C. J. *J. Am. Chem. Soc.* **2009**, *130*, 10998−11009.

(13) (a) Gaspar, A. B.; Seredyuk, M.; Gutlich, P. *Coord. Chem. Rev.* **2014**, *268*, 41−58. (b) Hayami, S.; Karim, M. R.; Lee, Y. H. *Eur. J. Inorg. Chem.* **2013**, 683−696. (c) Gaspar, A. B.; Seredyuk, M.; Gütlich, P. *Coord. Chem. Rev.* **2009**, *253*, 2399−2413.

(14) (a) Shepherd, H. J.; Molnár, G.; Nicolazzi, W.; Salmon, L.; Bousseksou, A. *Eur. J. Inorg. Chem.* **2013**, *2013*, 653−661. (b) Cavallini, M. *Phys. Chem. Chem. Phys.* **2012**, *14*, 11867−11876.

(15) (a) Ruiz, E. *Phys. Chem. Chem. Phys.* **2014**, *16*, 14−22. (b) Miyamachi, T.; Gruber, M.; Davesne, V.; Bowen, M.; Boukari, S.; Joly, L.; Scheurer, F.; Rogez, G.; Yamada, T. K.; Ohresser, P.;

DOI: 10.1021/acs.inorgchem.5b00978
Inorg. Chem. 2015, 54, 7906−7914

Beaurepaire, E.; Wulfhekel, W. *Nat. Commun.* **2012**, *3*, 938(1−6). (c) Gopakumar, T. G.; Matino, F.; Naggert, H.; Bannwarth, A.; Tuczek, F.; Berndt, R. *Angew. Chem., Int. Ed.* **2012**, *51*, 6262−6266.
(16) Ruaudel-Teixier, A.; Barraud, A.; Coronel, P.; Kahn, O. *Thin Solid Films* **1988**, *160*, 107−115.
(17) (a) Etrillard, C.; Faramarzi, V.; Dayen, J. F.; Lètard, J. F.; Doudin, B. *Chem. Commun.* **2011**, *47*, 9663−9665. (b) Tobon, Y. A.; Etrillard, C.; Nguyen, O.; Lètard, J. F.; Faramarzi, V.; Dayen, J. F.; Doudin, B.; Bassani, D. M.; Guillaume, F. *Eur. J. Inorg. Chem.* **2012**, *35*, 5837−5842.
(18) (a) Tissot, A.; Enachescu, C.; Boillot, M. L. *J. Mater. Chem.* **2012**, *22*, 20451−20457. (b) Bertoni, R.; Lorenc, M.; Tissot, A.; Servol, M.; Boillot, M. L.; Collet, E. *Angew. Chem., Int. Ed.* **2012**, *51*, 7485−7489. (c) Rotaru, A.; Gural'skiy, I. A.; Molnàr, G.; Salmon, L.; Demont, P.; Bousseksou, A. *Chem. Commun.* **2013**, *48*, 4163−4165.
(19) (a) Coronado, E.; Galán-Mascarós, J. R.; Monrabal-Capilla, M.; García-Martínez, J.; Pardo-Ibañez, P. *Adv. Mater.* **2007**, *19*, 1359−1361. (b) Létard, J.-F.; Daro, N.; Nguyen, O. Patent No. FR 0512476 (August 12, 2005) and Patent No. WO 2007/065996 (June 14, 2007). (c) Galán-Mascarós, J. R.; Coronado, E.; Forment-Aliaga, A.; Monrabal-Capilla, M.; Pinilla-Cienfuegos, E.; Ceolin, M. *Inorg. Chem.* **2010**, *49*, 5706−5714.
(20) Volatron, F.; Catala, L.; Riviere, E.; Gloter, A.; Stephan, O.; Mallah, T. *Inorg. Chem.* **2008**, *47*, 6584−6586.
(21) (a) Boldog, I.; Gaspar, A. B.; Martinez, V.; Pardo-Ibañez, P.; Ksenofontov, V.; Bhattacharjee, A.; Gütlich, P.; Real, J. A. *Angew. Chem., Int. Ed.* **2008**, *47*, 6433−6437. (b) Martinez, V.; Boldog, I.; Gaspar, A. B.; Ksenofontov, V.; Bhattacharjee, A.; Gütlich, P.; Real, J. A. *Chem. Mater.* **2010**, *22*, 4271−4281.
(22) (a) Forestier, T.; Kaiba, A.; Pechev, S.; Denux, D.; Guionneau, P.; Etrillard, C.; Daro, N.; Freysz, E.; Lètard, J. F. *Chem. - Eur. J.* **2009**, *15*, 6122−6130. (b) Forestier, T.; Mornet, S.; Daro, N.; Nishihara, T.; Mouri, S. I.; Tanaka, K.; Fouche, O.; Freysz, E.; Lètard, J. F. *Chem. Commun.* **2008**, 4327−4329. (c) Neville, S. M.; Etrillard, C.; Asthana, S.; Lètard, J. F. *Eur. J. Inorg. Chem.* **2010**, *2010*, 282−288.
(23) (a) Tokarev, A.; Salmon, L.; Guari, Y.; Molnár, G.; Bousseksou, A. *New J. Chem.* **2011**, *35*, 2081−2088. (b) Tokarev, A.; Salmon, L.; Guari, Y.; Nicolazzi, W.; Molnár, G.; Bousseksou, A. *Chem. Commun.* **2010**, *46*, 8011−8013. (c) Peng, H.; Tricard, S.; Félix, G.; Molnàr, G.; Nicolazzi, W.; Salmon, L.; Bousseksou, A. *Angew. Chem., Int. Ed.* **2014**, *53*, 10894−10898.
(24) Martinho, P. N.; Lemma, T.; Gildea, B.; Picardi, G.; Müller-Bunz, H.; Forster, R. J.; Keyes, T. E.; Redmond, G.; Morgan, G. G. *Angew. Chem., Int. Ed.* **2012**, *51*, 11995−11999.
(25) (a) Seredyuk, M.; Gaspar, A. B.; Ksenofontov, V.; Reiman, S.; Galyametdinov, Y.; Haase, W.; Rentschler, E.; Gütlich, P. *Chem. Mater.* **2006**, *18*, 2513−2519. (b) Matsuda, M.; Tajima, H. *Chem. Lett.* **2007**, *36*, 700−701. (c) Tissot, A.; Bardeau, J. F.; Riviere, E.; Brisset, F.; Boillot, M. L. *Dalton Trans.* **2010**, *39*, 7806−7812. (d) Nakamoto, A.; Kojima, N.; Liu, X. J.; Moritomo, Y.; Nakamura, A. *Polyhedron* **2005**, *24*, 2909−2912. (e) Chen, Y.; Ma, J. G.; Zhang, J. J.; Shi, W.; Cheng, P.; Liao, D. Z.; Yan, S. P. *Chem. Commun.* **2010**, *46*, 5073−5075. (f) Cavallini, M.; Bergenti, I.; Milita, S.; Kengne, J. C.; Gentili, D.; Ruani, G.; Salitros, I.; Meded, V.; Ruben, M. *Langmuir* **2011**, *27*, 4076−4081. (g) Cavallini, M.; Bergenti, I.; Milita, S.; Ruani, G.; Salitros, I.; Qu, Z. R.; Chandrasekar, R.; Ruben, M. *Angew. Chem., Int. Ed.* **2008**, *47*, 8596−8600. (h) Alam, M. S.; Stocker, M.; Gieb, K.; Müller, P.; Haryono, M.; Student, K.; Grohmann, A. *Angew. Chem., Int. Ed.* **2010**, *49*, 1159−1163. (i) Felix, G.; Abdul-Kader, K.; Mahfoud, T.; Gural'skiy, I. A.; Nicolazzi, W.; Salmon, L.; Molnàr, G.; Bousseksou, A. *J. Am. Chem. Soc.* **2011**, *133*, 15342−15345.
(26) (a) Cobo, S.; Molnár, G.; Real, J. A.; Bousseksou, A. *Angew. Chem., Int. Ed.* **2006**, *45*, 5786−5789. (b) Molnár, G.; Cobo, S.; Real, J. A.; Carcenac, F.; Daran, E.; Vieu, C.; Bousseksou, A. *Adv. Mater.* **2007**, *19*, 2163−2167. (c) Agustí, G.; Cobo, S.; Gaspar, A. B.; Molnár, G.; Moussa, N. O.; Szilágyi, P. A.; Pálfi, V.; Vieu, C.; Carmen Muñoz, M.; Real, J. A.; Bousseksou, A. *Chem. Mater.* **2008**, *20*, 6721−6732. (d) Bartual-Murgui, C.; Akou, A.; Salmon, L.; Molnár, G.; Thibault, C.; Real, J. A.; Bousseksou, A. *Small* **2011**, *7*, 3385−3391. (e) Otsubo, K.; Haraguchi, T.; Sakata, O.; Fujiwara, A.; Kitagawa, H. *J. Am. Chem. Soc.* **2012**, *134*, 9605−9608.
(27) (a) Soyer, H.; Dupart, E.; Gomez-Garcia, C. J.; Mingotaud, C.; Delhaès, P. *Adv. Mater.* **1999**, *11*, 382−384. (b) Roubeau, O.; Natividad, E.; Agricole, B.; Ravaine, S. *Langmuir* **2007**, *23*, 3110−3117.
(28) (a) Shi, S.; Schmerber, G.; Arabski, J.; Beaufrand, J. B.; Kim, D. J.; Boukari, S.; Bowen, M.; Kemp, N. T.; Viart, N.; Rogez, G.; Beaurepaire, E.; Aubriet, H.; Petersen, J.; Becker, C.; Ruch, D. *Appl. Phys. Lett.* **2009**, *95*, 043303. (b) Naggert, H.; Bannwarth, A.; Chemnitz, S.; von Hofe, T.; Quandt, E.; Tuczek, F. *Dalton Trans.* **2011**, *40*, 6364−6366.
(29) Jacob, H.; Kathirvel, K.; Petersen, F.; Strunskus, T.; Bannwarth, A.; Meyer, S.; Tuczek, F. *Langmuir* **2013**, *29*, 8534−8543.
(30) Gural'skiy, I.; Quintero, C. M.; Molnár, G.; Fritsky, I. O.; Salmon, L.; Bousseksou, A. *Chem. - Eur. J.* **2012**, *18*, 9946−9954.
(31) Larionova, J.; Salmon, L.; Guari, Y.; Tokarev, A.; Molvinger, K.; Molnàr, G.; Bousseksou, A. *Angew. Chem., Int. Ed.* **2008**, *47*, 8236−8240.
(32) (a) Raza, Y.; Volatron, F.; Moldovan, S.; Ersen, O.; Huc, V.; Martini, C.; Brisset, F.; Gloter, A.; Stephan, O.; Bousseksou, A.; Catala, L.; Mallah, T. *Chem. Commun.* **2011**, *47*, 11501−11503. (b) Faulmann, C.; Chahine, J.; Malfant, I.; de Caro, D.; Cormary, B.; Valade, L. *Dalton Trans.* **2011**, *40*, 2480−2485. (c) Durand, P.; Pillet, S.; Bendeif, E.; Carteret, C.; Bouazaoui, M.; El Hamzaoui, H.; Capoen, B.; Salmon, L.; Hébert, S.; Ghanbaja, J.; Aranda, L.; Schaniel, D. *J. Mater. Chem. C* **2013**, *1*, 1933−1942.
(33) (a) Madeja, K.; König, E. *J. Inorg. Nucl. Chem.* **1963**, *25*, 377−385. (b) Müller, E. W.; Spiering, H.; Gütlich, P. *Chem. Phys. Lett.* **1982**, *93*, 567−571. (c) Ganguli, P.; Güetlich, P.; Müeller, E. W. *Inorg. Chem.* **1982**, *21*, 3429−3433. (d) Gallois, B.; Real, J. A.; Hauw, C.; Zarembowitch, J. *Inorg. Chem.* **1990**, *29*, 1152−1158. (e) Cartier dit Moulin, C.; Rudolf, P.; Flank, A. M.; Chen, C. T. *J. Phys. Chem.* **1992**, *96*, 6196−6198. (f) Granier, T.; Gallois, B.; Gaultier, J.; Real, J. A.; Zarembowitch, J. *Inorg. Chem.* **1993**, *32*, 5305−5312. (g) Lee, J. J.; Sheu, H. S.; Lee, C. R.; Chen, J. M.; Lee, J. F.; Wang, C. C.; Huang, C. H.; Wang, Y. *J. Am. Chem. Soc.* **2000**, *122*, 5742−5747. (h) Paulsen, H.; Duelund, L.; Winkler, H.; Toftlund, H.; Trautwein, A. X. *Inorg. Chem.* **2001**, *40*, 2201−2203. (i) Marchivie, M.; Guionneau, P.; Howard, J. A. K.; Chastanet, G.; Lètard, J. F.; Goeta, A. E.; Chasseau, D. *J. Am. Chem. Soc.* **2002**, *124*, 194−195. (j) Gütlich, P.; Goodwin, H. A. *Top. Curr. Chem.* **2004**, *233*, 1−47. (k) Ksenofontov, V.; Gaspar, A. B.; Levchenko, G.; Fitzsimmons, B.; Gütlich, P. *J. Phys. Chem. B* **2004**, *108*, 7723−7727.
(34) Rasband, W. S. *ImageJ*; U.S. National Institutes of Health: Bethesda, MD, 1997−2007; http://rsb.info.nih.gov/ij/.
(35) (a) Ozin, G. A.; Arsenault, A. C. *Nanochemistry: A Chemical Approach to Nanomaterials*; The Royal Society of Chemistry: Cambridge, 2005. (b) Burda, C.; Chen, X.; Narayanan, R.; El-Sayed, M. A. *Chem. Rev.* **2005**, *105*, 1025−1102.
(36) Dézsi, I.; Molnár, B.; Tarnóczi, T.; Tompa, K. *J. Inorg. Nucl. Chem.* **1967**, *29*, 2486−2490.
(37) Gerasimova, T. P.; Katsyuba, S. A. *Dalton Trans.* **2013**, *42*, 1787−1797.
(38) (a) Tissot, A.; Enachescu, C.; Boillot, M. L. *J. Mater. Chem.* **2012**, *22*, 20451−20457. (b) Tanasa, R.; Laisney, J.; Stancu, A.; Boillot, M. L.; Enachescu, C. *Appl. Phys. Lett.* **2014**, *104*, 031909.

DOI: 10.1021/acs.inorgchem.5b00978
Inorg. Chem. 2015, 54, 7906−7914